Loss of perivascular aquaporin 4 may underlie deficient water and K^+ homeostasis in the human epileptogenic hippocampus

Tore Eid*[†‡§], Tih-Shih W. Lee[‡¶], Marion J. Thomas[‖**], Mahmood Amiry-Moghaddam[‖**], Lars P. Bjørnsen*[‖], Dennis D. Spencer*, Peter Agre[‡‡], Ole P. Ottersen[‖**], and Nihal C. de Lanerolle*

Departments of *Neurosurgery, [†]Laboratory Medicine, and [¶]Psychiatry, Yale University School of Medicine, New Haven, CT 06520; [‖]Centre for Molecular Biology and Neuroscience and Centre for Water Imbalance-Related Disorders and **Department of Anatomy, University of Oslo, N-0316 Oslo, Norway; and [††]Departments of Biological Chemistry and Medicine, The Johns Hopkins University School of Medicine, Baltimore, MD 21205

Contributed by Peter Agre, December 17, 2004

An abnormal accumulation of extracellular K^+ in the brain has been implicated in the generation of seizures in patients with mesial temporal lobe epilepsy (MTLE) and hippocampal sclerosis. Experimental studies have shown that clearance of extracellular K^+ is compromised by removal of the perivascular pool of the water channel aquaporin 4 (AQP4), suggesting that an efficient clearance of K^+ depends on a concomitant water flux through astrocyte membranes. Therefore, we hypothesized that loss of perivascular AQP4 might be involved in the pathogenesis of MTLE. Whereas Western blot analysis showed an overall increase in AQP4 levels in MTLE compared with non-MTLE hippocampi, quantitative ImmunoGold electron microscopy revealed that the density of AQP4 along the perivascular membrane domain of astrocytes was reduced by 44% in area CA1 of MTLE vs. non-MTLE hippocampi. There was no difference in the density of AQP4 on the astrocyte membrane facing the neuropil. Because anchoring of AQP4 to the perivascular astrocyte endfoot membrane depends on the dystrophin complex, the localization of the 71-kDa brain-specific isoform of dystrophin was assessed by immunohistochemistry. In non-MTLE hippocampus, dystrophin was preferentially localized near blood vessels. However, in the MTLE hippocampus, the perivascular dystrophin was absent in sclerotic areas, suggesting that the loss of perivascular AQP4 is secondary to a disruption of the dystrophin complex. We postulate that the loss of perivascular AQP4 in MTLE is likely to result in a perturbed flux of water through astrocytes leading to an impaired buffering of extracellular K^+ and an increased propensity for seizures.

dystrophin | epilepsy | seizures | astrocytes

Mesial temporal lobe epilepsy (MTLE) is one of the commonest forms of medically intractable epilepsies. MTLE is characterized by seizures that originate from mediobasal temporal lobe structures, particularly the hippocampus, and neurosurgical resection of the epileptogenic hippocampus is often used to treat this disorder. The resected, epileptogenic hippocampus in MTLE is typically indurated and atrophic and displays massive loss of neurons along with astroglial changes, particularly in areas CA1 and CA3 and the dentate hilus, a condition known as hippocampal (or Ammon's horn) sclerosis. Electrophysiological recordings from MTLE hippocampi have demonstrated that these hippocampi are hyperexcitable when compared with non-sclerotic hippocampi from patients with other types of temporal lobe epilepsy, such as mass associated temporal lobe epilepsy (patients with an extrahippocampal mass lesion) or paradoxical temporal lobe epilepsy (patients without a mass lesion and with seizures of unknown etiology). A fundamental question that remains to be resolved is why the MTLE hippocampus is hyperexcitable.

Studies of MTLE patient hippocampi have shown that the K^+ buffering capacity is diminished when compared with non-MTLE hippocampi (1). This decrease is most pronounced in sclerotic areas of the hippocampus, such as CA1, where patch clamp experiments have demonstrated impaired uptake of K^+ into astrocytes by means of inwardly rectifying K^+ channels (2, 3). The sclerotic, MTLE hippocampus also exhibits increased T2 signal density on magnetic resonance imaging and higher than normal apparent diffusion coefficient on diffusion-weighted imaging, suggesting that water accumulates in this structure (4). Moreover, the expression of mRNA for aquaporin 4 (AQP4) is increased in area CA1 of MTLE hippocampi compared with non-MTLE hippocampi (5).

Loss of AQP4 from the perivascular endfoot domain of astrocytes is associated with reduced clearance of extracellular K^+ and increased severity of seizures in an animal model of α-syntrophin deletion (6). This and other studies (7, 8) suggest that buffering of K^+ by means of inwardly rectifying K^+ channels on astrocytes depends on a parallel flux of water through the plasma membrane of these cells. Under conditions of high neuronal activity, K^+ and water are taken up by the astrocyte membrane facing the neuropil and siphoned into blood or cerebrospinal fluid through the endfoot membrane (9). Thus, in experimental models, a perturbation of the flux of K^+ and water exacerbates the potential for seizures. Here, we present data suggesting that a similar mechanism may operate in the hippocampus of patients with MTLE.

Materials and Methods

Tissue. Patients with medically intractable temporal lobe epilepsy underwent phased presurgical evaluation at the Yale–New Haven Hospital, and those selected for surgery had their hippocampus resected according to standard procedures (10). During the period of July 1996 to February 2002, a total of 86 hippocampi were resected. Twenty-four of these hippocampi were randomly selected for the present study, and they are therefore representative of the patient population that undergoes surgery at Yale. Informed consent from each patient and institutional approval were obtained for the use of tissue in this project (see Table 1).

Classification. Tissue classification was carried out separately by two investigators (T.E. and N.C.d.L.), and the samples were encoded for further use. Thus, the investigators performing the Western blots (M.J.T. and M.A.-M.) and quantitative electron microscopy (L.P.B.) were unaware of the patient categories until the experiments had been completed and the data were ready for statistical analysis.

Abbreviations: MTLE, mesial temporal lobe epilepsy; AQP4, aquaporin 4.

[‡]T.E. and T.-S.W.L. contributed equally to this work.

[§]To whom correspondence should be addressed at: Department of Neurosurgery, Yale University School of Medicine, 333 Cedar Street, P.O. Box 208082, New Haven, CT 06520-8082. E-mail: tore.eid@yale.edu.

Table 1. Characteristics of patients selected for the study

Case	Gender	Age, years	Years since first unprovoked seizure	AEDs at surgery	MRI findings	Pathology	Classification
1	M	39	16	ltg	Unremarkable	Unremarkable	Non-MTLE
2	F	22	10	tpm	Unremarkable	Unremarkable	Non-MTLE
3	F	46	28	cbz	Unremarkable	Unremarkable	Non-MTLE
4	M	40	4	lev, vpa	Unremarkable	Unremarkable	Non-MTLE
5	M	44	18	cbz, clo	R hippocampal sclerosis	Unremarkable	Non-MTLE
6	F	49	42	lev	Chiari I malformation; otherwise unremarkable	Unremarkable	Non-MTLE
7	F	38	30	cbz, tpm	Unremarkable	Unremarkable	Non-MTLE
8	M	35	17	ltg, cbz	Cavernous hemangioma, R amygdala, adjacent to hippocampal head; normal hippocampus	Cavernous hemangioma	Non-MTLE
9	M	27	1	cbz	L mesial temporal lobe mass lesion encroaching subbasal ganglia, replacing and involving amygdala and anterior hippocampus	Oligodendroglioma	Non-MTLE
10	F	10	5	ltg	R temporal lobe tumor involving basal ganglia and amygdala; bilateral hippocampal atrophy.	Low-grade astrocytoma	Non-MTLE
11	F	8	4	cbz	L temporal lobe tumor	Oligodendroglioma	Non-MTLE
12	M	47	22	cbz	R hippocampal atrophy	Hippocampal sclerosis	MTLE
13	F	36	14	cbz	L hippocampal sclerosis	Hippocampal sclerosis	MTLE
14	F	45	27	cbz, pri, gpn	R hippocampal atrophy	Hippocampal sclerosis	MTLE
15	M	40	39	cbz, pht	Unremarkable	Hippocampal sclerosis	MTLE
16	M	27	26	gpn, flb	R hippocampal atrophy	Hippocampal sclerosis	MTLE
17	M	24	16	tpm, pb	R hippocampal atrophy	Hippocampal sclerosis	MTLE
18	F	28	19	cbz	L hippocampal atrophy	Hippocampal sclerosis	MTLE
19	F	15	10	cbz, ltg	L hippocampal sclerosis with increased signal on FLAIR	Hippocampal sclerosis	MTLE
20	F	50	40	cbz	L hippocampal sclerosis with increased signal on FLAIR; bilateral small vessel ischemic changes	Hippocampal sclerosis	MTLE
21	F	36	26	ltg, pri	R hippocampal sclerosis with increased signal on FLAIR	Hippocampal sclerosis	MTLE
22	F	39	12	gpn, ltg	R hippocampal sclerosis	Hippocampal sclerosis	MTLE
23	M	46	10	ltg, lev	R hippocampal sclerosis	Hippocampal sclerosis	MTLE
24	F	51	33	cbz	L hippocampal sclerosis	Hippocampal sclerosis	MTLE

For non-MTLE, $n = 11$, and for MTLE, $n = 13$. M, male; F, female; AEDs, antiepileptic drugs; cbz, carbamazepine; clo, clonazepam; flb, felbamate; pht, phenytoin; lev, levetiracetam; li, lithium; ltg, lamotrigine; gpn, gabapentin; pb, phenobarbial; pri, primidone; tpm, topiramate; vpa, valproate; L, left; R, right; FLAIR, fluid-attenuated inversion recovery imaging.

The surgically resected hippocampi were classified into two groups (see ref. 11 for details): MTLE (group 1) and non-MTLE (group 2). In MTLE, the seizure activity is believed to originate from the hippocampus based on noninvasive studies, depth, and/or subdural electrode recordings. The MTLE hippocampus is characterized by pronounced neuronal loss (>50%) and extensive astroglial proliferation in the hippocampal subfields CA1, CA3, and hilus. Also, this category shows reorganization of peptidergic (dynorphin, somatostatin, neuropeptide Y, and substance P) neurons in the dentate gyrus. The non-MTLE hippocampi are recognized by a modest (<25%) neuronal loss throughout all hippocampal subfields, minimal astroglial proliferation, and no reorganization of peptidergic neurons in the dentate gyrus. The histological pattern in the non-MTLE hippocampi is similar to that of autopsy hippocampi. In ≈50% of the non-MTLE hippocampi, the seizures are thought to originate from a mass lesion (usually a tumor) outside the hippocampus but within the temporal lobe territory. In the remaining cases, no mass lesion is apparent and the hippocampi are selected for resection based on intracranial recordings of seizure onset.

Tissue Preparation. Immediately after surgical resection, two 5-mm-thick slices were cut from the center portion of the hippocampus. One of the samples was immersed into a fixative containing 4% paraformaldehyde and 15% (vol/vol) saturated picric acid in 0.1 M phosphate buffer, pH 7.4, for 1 h, followed by immersion into 5% acrolein in phosphate buffer, pH 7.4, for 3 h. Fifty-micrometer coronal sections were cut on a Vibratome and either (*i*) stored in a cryoprotection solution (FD NeuroTechnologies, Catonsville, MD) at −80°C until processed for preembedding immunohistochemistry or (*ii*) processed immediately for freeze substitution. The other sample was rapidly frozen on dry ice and cut coronally into 200-μm sections on a cryostat and stored at −80°C until used for Western blotting.

Antisera and Chemicals. Affinity-purified polyclonal (rabbit) antibodies against AQP4 (Chemicon) and monoclonal (mouse) antibodies against dystrophin (NovoCastra, Newcastle upon Tyne, U.K.) were used. The dystrophin antibody was made against a synthetic polypeptide consisting of the last 17 aa of the carboxyl terminus of the human dystrophin sequence (SSRGRNTPGKPMREDTM). This sequence is present in the astrocyte-specific form of dystrophin, Dp71 (12). Unless otherwise specified, all other chemicals were obtained from Sigma–Aldrich.

Western Blotting. Frozen non-MTLE and MTLE whole hippocampi were sonicated on ice in homogenization buffer (50

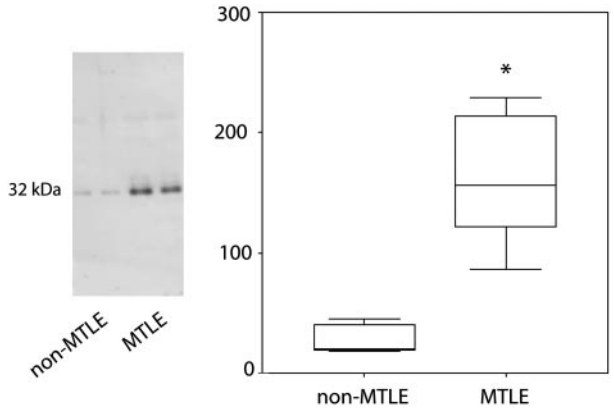

Fig. 1. There is an overall increase in AQP4 protein in the MTLE hippocampus. Western blots of representative non-MTLE and MTLE patient hippocampi immunostained with antibodies against AQP4 reveal single bands at the expected molecular mass of 32 kDa. The band intensities from six randomly selected non-MTLE and MTLE hippocampi (total of 12) were determined and visualized by box plots. The value of the *y* axis is the labeling intensity of AQP4 compared with a standard control of neocortical tissue (see *Materials and Methods* for details). A 360% increase in labeling intensity for AQP4 is evident in MTLE vs. non-MTLE (*, $P = 0.002$, two-tailed Mann–Whitney *U* test).

mM 3-[*N*-morpholino]propane-sulfonic acid·HCl/2 mM DTT, pH 7.6/3 mM EGTA/0.5 mM magnesium acetate/0.1 mM sodium orthovanadate/0.1 mM PMSF/20 μg/ml leupeptin/10 μg/ml pepstatin A/5 μg/ml aprotinin/0.32 M sucrose). Protein concentrations were determined with a BCA Protein Assay kit (Pierce). After being diluted in a sample loading buffer (50% sucrose/7.5% SDS/62.5 mM Tris, pH 6.8/2 mM EDTA/3.1% DTT/0.01% bromophenol blue), 10 μg of protein was added per lane, separated by electrophoresis on 12% polyacrylamide gels (MiniProtean II, Bio-Rad) and transferred onto poly(vinylidene difluoride) membranes. Membranes were blocked for 1 h in Tris-buffered saline (20 mM Tris/137 mM NaCl, pH 7.6) plus 0.1% Tween 20 (TBS-T) plus 5% blocking agent [Enhanced Chemifluorescence (ECH) kit, Amersham Biosciences], followed by overnight incubation in primary antibody (1 μg/ml AQP4; catalog no. AB3068, Chemicon). Membranes were subsequently incubated for 1 h in fluorescein-conjugated anti-rabbit antibodies (ECF kit, diluted 1:600), followed by a 1-h incubation in alkaline phosphatase-conjugated anti-fluorescein antibody (ECF kit, diluted 1:2,500). All steps were carried out at room temperature with antibodies diluted in TBST plus 1% milk powder.

After each incubation, membranes were washed in TBS-T. The chemifluorescent signal was detected with a laser scanner (Molecular Imager FX, Bio-Rad). For each blot, a global background subtraction was performed that removed the high-frequency, low-intensity pixels. After magnification, individual pixels were visible, and each band was traced manually by using the same background pixel intensity immediately adjacent to the band as a cutoff. Similarly, a standard curve was constructed for each blot with increasing concentrations (within the linear range of the curve) of SDS-homogenized human neocortex from a non-MTLE patient, with the highest concentration set at 100%. The volume values (volume = sum of intensities of the pixels within the volume boundary × pixel area) of the bands were determined for AQP4 and the relative concentrations from the patient samples were determined by comparison with the standard curve.

Preembedding Immunohistochemistry for Light Microscopy. Vibratome sections were processed free-floating according to the avidin–biotin complex method of Hsu *et al*. (13) as described in ref. 14 with the following modifications: Incubation in the primary antibodies was done for 18 h at room temperature at dilutions of 1:10,000 for anti-AQP4 and 1:5,000 for anti-dystrophin; a commercially available kit (VECTASTAIN Elite, Vector Laboratories) was used for the remaining procedure.

Freeze Substitution. Small tissue blocks ($0.3 \times 0.5 \times 1$ mm^3) of area CA1 were dissected from the 500-μm Vibratome sections and subjected to freeze substitution (15). Briefly, the tissue blocks were cryoprotected in glycerol and rapidly frozen in liquid propane at −190°C. The frozen tissue was immersed into anhydrous methanol containing 0.5% uranyl acetate at −90°C in an automatic freeze substitution unit (EMAFS, Leica, Vienna, Austria). The blocks were infiltrated with Lowicryl HM20 Resin (Lowi, Waldkraiburg, Germany) at −30°C, polymerized by UV light, sectioned at 60 nm, transferred to 500-mesh nickel grids, and processed for ImmunoGold electron microscopy.

Postembedding ImmunoGold Electron Microscopy and Specificity Controls. On-grid immunolabeling of AQP4 was carried out in six non-MTLE and six MTLE cases according to the procedure of Laake *et al*. (16) with some modifications. Briefly, the sections were incubated for 2 h or overnight with the AQP4 antiserum (raised in rabbit) diluted 1:100, followed by incubation for 2 h with 10-nm colloidal gold-conjugated secondary antibodies to rabbit IgG diluted 1:20 (EMGFAR, BB International, Cardiff,

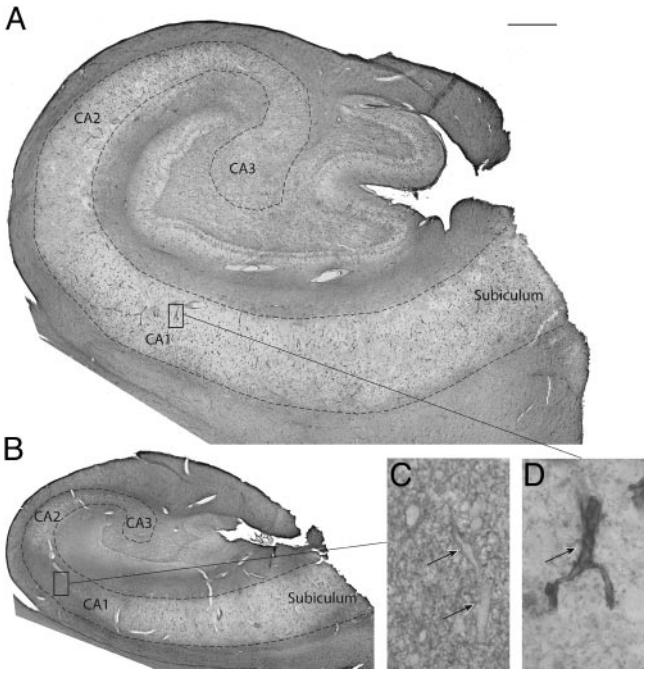

Fig. 2. Although AQP4 is preferentially distributed around blood vessels in the non-MTLE hippocampus, this localization is lost in MTLE. AQP4 is demonstrated by preembedding immunohistochemistry on Vibratome sections of a representative non-MTLE (*A* and *D*) and MTLE (*B* and *C*) hippocampus. (*A*) In the non-MTLE hippocampus, immunoreactivity for AQP4 in the pyramidal layer of Ammon's horn (the area within the dashed line) is preferentially distributed around blood capillaries. (Scale bar, 1 mm.) (*D*) This finding is demonstrated in the high-power field of CA1, where the arrow indicates a strongly immunopositive capillary amidst a weakly labeled neuropil. (Magnification, ×6 selected portion of *A*.) (*B*) In the MTLE hippocampus, the preferential distribution of AQP4 around blood capillaries is lost in the pyramidal layer in areas of sclerosis (such as CA1). Scale is the same as in *A*. (*C*) In the high-power field of CA1 moderate immunolabeling for AQP4 is present throughout the neuropil and also around blood capillaries, which are indicated by arrows. (Magnification, ×6 selected portion of *B*.)

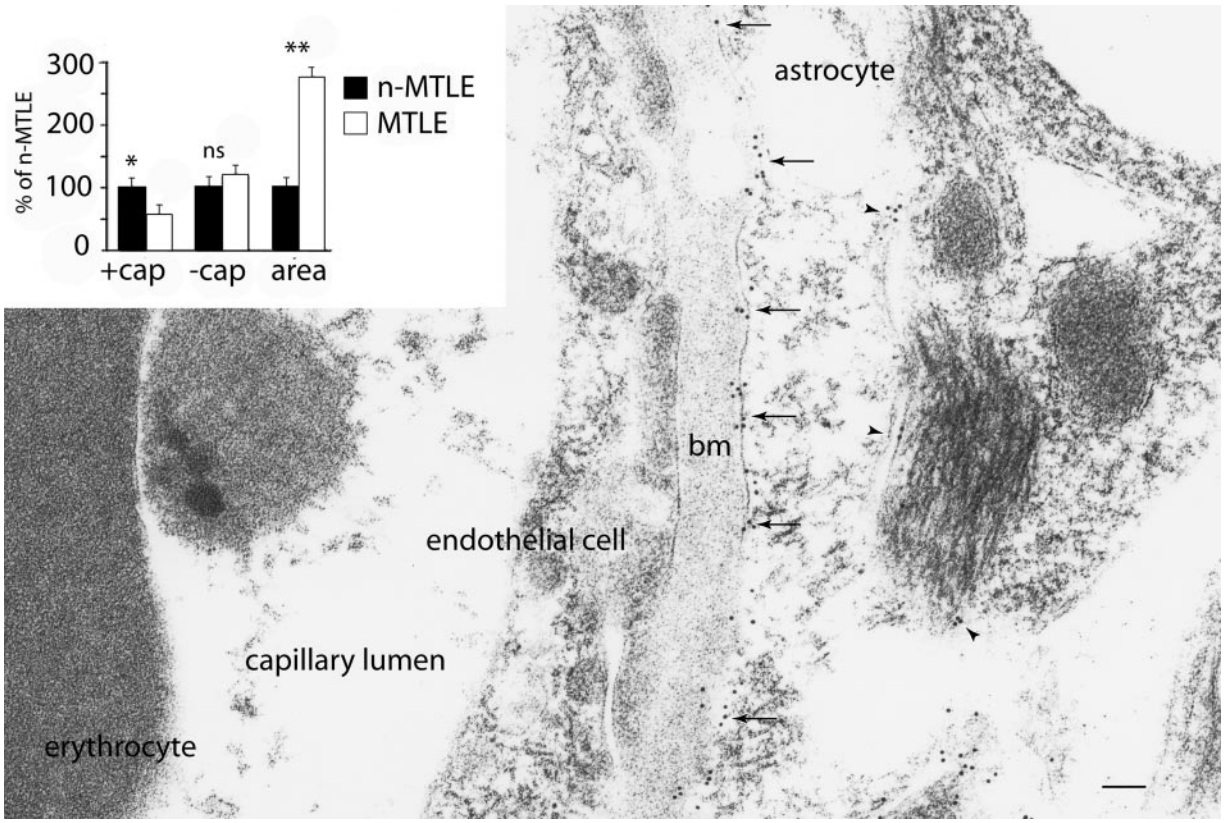

Fig. 3. Quantitative ImmunoGold electron microscopy reveals significant loss of AQP4 from the perivascular astrocyte membrane in MTLE vs. non-MTLE hippocampi. ImmunoGold electron microscopy of the endothelial–astrocyte interface in CA1 of a representative non-MTLE hippocampus demonstrates that AQP4 (arrows) is enriched on the astrocyte membrane facing the endothelial cell. Considerably less labeling is present on the astrocyte membrane facing the neuropil (arrowheads). (*Inset*) Quantitation of gold particle densities in random fields from area CA1 of six non-MTLE (n-MTLE) and six MTLE hippocampi. Gold particle counts for MTLE are given as percent of non-MTLE ± SEM: astrocyte membranes facing the endothelial cell (+cap; particles per μm), 56 ± 16% (*, P = 0.01); astrocyte membranes facing the neuropil (−cap; particles per μm), no change. The number of gold particles per unit area of neuropil (particles per μm^2) was 273 ± 23% (**, P = 0.013). A two-tailed Mann–Whitney U test was used for statistical analysis. bm, basal lamina; ns, not significant. (Scale bar, 100 nm.)

U.K.). The sections were counterstained with uranyl acetate followed by lead citrate or lead nitrate before being examined in a transmission electron microscope (Jeol EM 300). Substitution of the primary antibodies with normal serum or preimmune sera completely abolished the staining.

Statistical Analysis. A two-tailed Mann–Whitney U test was used to examine the differences in the Western blot results. In the postembedding experiments, gold particle densities were calculated per unit plasma membrane of randomly selected astrocyte profiles that were facing (*i*) the perivascular compartment or (*ii*) the neuropil. Gold particles were included in the counts as long as they touched the membrane, even if their center of gravity projected outside the plasma membrane. In addition, the total number of gold particles per unit area was calculated from particle counts in five randomly selected areas (total ≈60 μm^2) of the neuropil from each patient. Analysis was performed on electron micrographs that were digitized and analyzed by the Neurolucida system (Microbrightfield, Burlington, VT). Gold particle counts from six non-MTLE and six MTLE patients were used in the analysis.

Results

The level of AQP4 protein in hippocampal specimens from six non-MTLE and six MTLE patients was assessed by quantitative Western blotting. AQP4 was elevated by 360% in MTLE than in non-MTLE (P = 0.002, two-tailed Mann–Whitney U test) (Fig. 1). This finding is in accord with RT-PCR experiments of patient hippocampi in which the content of AQP4 mRNA is elevated by 257% in MTLE vs. non-MTLE (5). The increase in AQP4 in MTLE is proportional to the increase in the astrocyte marker glial fibrillary acidic protein (5); thus, the overall increase in AQP4 in MTLE can be explained by the proliferation of astrocytes typical of hippocampal sclerosis.

Immunocytochemistry was carried out to determine whether the increase in AQP4 was associated with a subcellular redistribution of AQP4. Light microscopic analysis revealed that AQP4 was enriched near blood vessels in non-MTLE hippocampi, consistent with a preferential localization of AQP4 in the perivascular endfeet of astrocytes (n = 11) (Fig. 2 *A* and *D*). In CA1 of the MTLE hippocampus (n = 13), the perivascular localization of AQP4 was disrupted (Fig. 2 *B* and *C*). Detailed analysis by ImmunoGold electron microscopy confirmed that the AQP4 labeling was confined to the plasma membrane of astrocytes in non-MTLE (n = 6) (Fig. 3) and MTLE (n = 6) hippocampi. Quantitation revealed that the labeling density was reduced by 44% on the perivascular astrocyte membrane in MTLE vs. non-MTLE (Fig. 3) hippocampi. In contrast, the labeling density of the astrocyte membrane facing the neuropil was the same in both patient categories. As expected from the increased number of astrocyte profiles in MTLE the gold particle density per unit area in randomly selected fields of the neuropil was 173% higher in MTLE hippocampi than in non-MTLE hippocampi (Fig. 3).

Anchoring of AQP4 to the perivascular astrocyte endfoot membrane depends on interactions with proteins of the dystro-

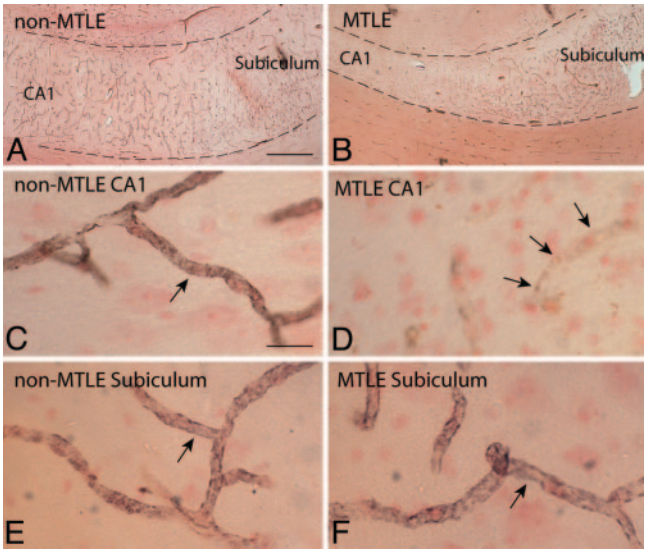

Fig. 4. Loss of perivascular AQP4 in the MTLE hippocampus is associated with a deficiency in perivascular dystrophin. Adjacent sections from the non-MTLE (*A*, *C*, and *E*) and MTLE (*B*, *D*, and *F*) hippocampi shown in Fig. 1 were immunolabeled with an antibody against the astrocyte-specific isoform of dystrophin (Dp71) and counterstained with neutral red. (*A* and *B*) The low-power micrographs from non-MTLE (*A*) and MTLE (*B*) depict the CA1-subiculum-transition, with the pyramidal layer between the dashed lines. (Scale bar, 500 μm.) (*C*, *D*, and *E*) In CA1 (*C*) and subiculum (*E*) of the non-MTLE hippocampus, there is strong immunolabeling for dystrophin around blood capillaries (arrows in *C* and *E*), whereas in the MTLE hippocampus, pericapillary immunolabeling for dystrophin is reduced in CA1 (arrows in *D*). (Scale bars, 40 μm.) (*F*) The validity of this finding is attested by the presence of numerous strongly dystrophin-positive capillaries in the subiculum of MTLE. (Scale bar, 40 μm.)

phin complex (17). Notably, deficiency in either dystrophin (18) or α-syntrophin (6) leads to loss of perivascular AQP4. Moreover, patients with Becker muscular dystrophy, a disorder characterized by defective expression of dystrophin, have increased incidence of epilepsy (19). In a recent microarray analysis of mRNA expression of nine dystrophin-associated proteins, only dystrophin was significantly lower by 68% in MTLE vs. non-MTLE hippocampi, whereas α-syntrophin mRNA was unchanged (5). To evaluate whether the deficiency of dystrophin in MTLE is related to the redistribution of AQP4, we localized dystrophin by immunohistochemistry with an antibody against the carboxyl terminus of the molecule. This antibody recognizes the 71-kDa major brain dystrophin isoform, Dp71, which is expressed in astrocytes (20). In agreement with animal studies, in the non-MTLE hippocampus, the immunolabeling for dystrophin was preferentially localized near blood vessels throughout all hippocampal subfields (Fig. 4 *A*, *C*, and *E*). In the MTLE hippocampus, the perivascular labeling for dystrophin was reduced in sclerotic areas (e.g., CA1) (Fig. 4 *B*, *D*, and *F*), despite the presence of numerous blood vessels in the latter (data not shown). In nonsclerotic areas of the MTLE hippocampus (Fig. 4 *B* and *F*), the labeling for dystrophin was similar to that of non-MTLE hippocampi (Fig. 4 *A* and *E*).

Discussion

As pointed out in the Introduction, hippocampi removed from patients with MTLE show evidence of an impaired water and K^+ homeostasis (1–3). This finding has obvious pathophysiological implications, because any buildup of K^+ in the extracellular space would increase neuronal excitability and contribute to the epileptogenicity of the relevant hippocampal subfields (21, 22). A reduced capacity to handle excess K^+ is likely to be particularly deleterious once a seizure has been precipitated. In such a situation a loss of K^+ homeostasis could easily set up a vicious cycle leading to a prolongation and aggravation of the epileptic seizures (23).

According to experimental studies, the processes responsible for clearance of extracellular K^+ are compromised by removing perivascular AQP4 (6). The most parsimonious interpretation of the latter observation is that K^+ homeostasis depends on the integrity of the mechanisms that are responsible for water flux through the perivascular astrocyte membrane. Functionally, the perivascular membrane domain is coupled in series with the astrocyte membrane domain that faces the neuropil and is likely to be critically involved in mediating water and K^+ efflux from the extracellular space surrounding active synapses (6). Corroborating the functional coupling between water transport and K^+ clearance, it has long been known that synaptic activation causes not only an increase in extracellular K^+ but also a decrease in extracellular space volume (24, 25). The exact mechanism underlying the coupling between K^+ and water transport is not known, but it has been proposed that the two transport processes are coupled through the activation of glial bicarbonate uptake (26). What is clear is that K^+ is not fluxed through AQP4 itself because AQP4 shows no evidence of a K^+ conductance in experimental models (27).

Mice lacking perivascular AQP4 after the removal of the anchoring protein α-syntrophin do not show any reduction in the total level of AQP4 in brain tissue (28). Quantitative electron microscopical studies have provided an explanation of this finding: The loss of AQP4 from the perivascular membrane domain is compensated for by a sustained or increased complement of AQP4 in the remainder of the astrocyte plasma membrane (28). Our previous finding that the brains of these mice display obvious deficiencies in water and K^+ transport underlines the fact that astrocytes are functionally polarized and that their normal function depends on a correct compartmentation of their membrane molecules (6). Specifically, the mislocalization of AQP4 induced by α-syntrophin deletion interferes with homeostatic processes that require a serial coupling between endfeet and non-endfeet astrocyte plasma membranes (29).

The question addressed in the present study is whether epileptogenic hippocampi from patients with MTLE display a mislocalization of AQP4 similar to that found to be associated with increased seizure vulnerability in transgenic mice. Our data indeed show that MTLE tissue mimics tissue from $syn^{-/-}$ animals by displaying a reduced density of AQP4 in perivascular membranes. Moreover, as in $syn^{-/-}$ animals, the tissue level of AQP4 is not decreased but significantly increased.

The most pressing question is whether the changes observed are responsible for the observed loss of K^+ and water homeostasis in the epileptogenic hippocampus. Extrapolation from the transgenic studies discussed above suggests that such a mechanistic coupling may exist. For obvious reasons this question cannot be subjected to direct experimental testing. It should be pointed out, however, that the present study provides the first evidence that a perturbed expression pattern of a membrane molecule could underlie the deficiency in water and K^+ homeostasis in MTLE. Whether other molecular mechanisms also contribute will have to be resolved in future studies.

What could be the mechanism underlying the loss of perivascular AQP4 in MTLE hippocampi? That this loss reflects a general depletion of AQP4 is ruled out by the finding that the tissue level of AQP4 increases rather than decreases. It was logical to look for changes in the dystrophin complex, which is known to be responsible for anchoring of AQP4 at perivascular membranes (17). Specifically, we tested whether tissue deficient in perivascular AQP4 showed a concomitant loss of perivascular DP71, the major dystrophin isoform in the brain (20). The finding that AQP4 and DP71 were similarly mislocalized suggests that the loss of perivas-

cular AQP4 may be secondary to a dissolution of the dystrophin complex. One possible mechanism underlying a dissolution of this complex is activation of extracellular proteases (such as metalloproteinases) that could sever the coupling to the laminin of the perivascular basal lamina that normally keeps the dystrophin/aquaporin complex in place (30, 31). Activation of extracellular metalloproteinases is a common pathophysiological response e.g., to infections and stroke in the CNS (32).

Based on the present findings, we conclude that mislocalization of AQP4 might contribute to the epileptogenicity of the MTLE hippocampi. This conclusion does not necessarily mean that the changes observed are primary events in the pathogenesis of MTLE. It could well be that the mislocalization develops rather late in the sequence of events that culminates in epilepsy. However, the changes are not merely a trivial consequence of gliosis, given that they are not reproduced in gliosis associated with other pathological conditions (33). Irrespective of the temporal course of events, our findings have identified a molecular mechanism that could be targeted pharmacologically to reduce brain excitability.

We thank Ms. Ilona Kovacs for excellent technical assistance and Dr. Jung Kim for providing neuropathological diagnoses of brain tumors in the non-MTLE patients. This work was supported by National Institutes of Health Grants NS 048434 (to N.C.d.L.) and HL48268 and EY11239 (to P.A.) and by the European Cooperation in Scientific and Technological Research, the Norwegian Research Council, and the Nordic Council through the establishment of the Center for Water Imbalance-Related Disorders (to O.P.O.).

1. Bordey, A. & Sontheimer, H. (1998) *Epilepsy Res.* **32,** 286–303.
2. Hinterkeuser, S., Schroder, W., Hager, G., Seifert, G., Blumcke, I., Elger, C. E., Schramm, J. & Steinhauser, C. (2000) *Eur. J. Neurosci.* **12,** 2087–2096.
3. Schroder, W., Hinterkeuser, S., Seifert, G., Schramm, J., Jabs, R., Wilkin, G. P. & Steinhauser, C. (2000) *Epilepsia* **41,** Suppl. 6**,** S181–S184.
4. Hugg, J. W., Butterworth, E. J. & Kuzniecky, R. I. (1999) *Neurology* **53,** 173–176.
5. Lee, T., Eid, T., Mane, S., Kim, J. H., Spencer, D. D., Ottersen, O. P. & de Lanerolle, N. C. (2004) *Acta Neuropath. (Berlin)* **108,** 493–502.
6. Amiry-Moghaddam, M., Williamson, A., Palomba, M., Eid, T., de Lanerolle, N. C., Nagelhus, E. A., Adams, M. E., Froehner, S. C., Agre, P. & Ottersen, O. P. (2003) *Proc. Natl. Acad. Sci. USA* **100,** 13615–13620.
7. Niermann, H., Amiry-Moghaddam, M., Holthoff, K., Witte, O. W. & Ottersen, O. P. (2001) *J. Neurosci.* **21,** 3045–3051.
8. Holthoff, K. & Witte, O. W. (1996) *J. Neurosci.* **16,** 2740–2749.
9. Paulson, O. B. & Newman, E. A. (1987) *Science* **237,** 896–898.
10. Spencer, D. D. & Spencer, S. S. (1991) *Surgery for Epilepsy* (Blackwell, Boston).
11. de Lanerolle, N. C., Kim, J. H., Williamson, A., Spencer, S. S., Zaveri, H. P., Eid, T. & Spencer, D. D. (2003) *Epilepsia* **44,** 677–687.
12. Lidov, H. G. (1996) *Brain Pathol.* **6,** 63–77.
13. Hsu, S., Raine, L. & Fanger, H. (1981) *J. Histochem. Cytochem.* **29,** 577–580.
14. de Lanerolle, N. C., Brines, M. L., Kim, J. H., Williamson, A., Philips, M. F. & Spencer, D. D. (1992) in *Molecular Neurobiology of Epilepsy*, eds. Engel, J., Jr., Wasterlain, C., Cavalheiro, E. A., Heinemann, U. & Avanzini, G. (Elsevier, Amsterdam), pp. 205–220.
15. Hjelle, O. P., Chaudhry, F. A. & Ottersen, O. P. (1994) *Eur. J. Neurosci.* **6,** 794–804.
16. Laake, J. H., Takumi, Y., Eidet, J., Torgner, I. A., Roberg, B., Kvamme, E. & Ottersen, O. P. (1999) *Neuroscience* **88,** 1137–1151.
17. Neely, J. D., Amiry-Moghaddam, M., Ottersen, O. P., Froehner, S. C., Agre, P. & Adams, M. E. (2001) *Proc. Natl. Acad. Sci. USA* **98,** 14108–14113.
18. Vajda, Z., Pedersen, M., Fuchtbauer, E. M., Wertz, K., Stodkilde-Jorgensen, H., Sulyok, E., Doczi, T., Neely, J. D., Agre, P., Frokiaer, J. & Nielsen, S. (2002) *Proc. Natl. Acad. Sci. USA* **99,** 13131–13136.
19. Goodwin, F., Muntoni, F. & Dubowitz, V. (1997) *Eur. J. Paediatr. Neurol.* **1,** 115–119.
20. Chelly, J., Hamard, G., Koulakoff, A., Kaplan, J. C., Kahn, A. & Berwald-Netter, Y. (1990) *Nature* **344,** 64–65.
21. Traynelis, S. F. & Dingledine, R. (1988) *J. Neurophysiol.* **59,** 259–276.
22. Moody, W. J., Futamachi, K. J. & Prince, D. A. (1974) *Exp. Neurol.* **42,** 248–263.
23. McNamara, J. O. (1994) *J. Neurosci.* **14,** 3413–3425.
24. Lux, H. D., Heinemann, U. & Dietzel, I. (1986) *Adv. Neurol.* **44,** 619–639.
25. Dietzel, I., Heinemann, U., Hofmeier, G. & Lux, H. D. (1980) *Exp. Brain Res.* **40,** 423–432.
26. Nagelhus, E. A., Mathiisen, T. M. & Ottersen, O. P. (2004) *Neuroscience* **129,** 905–913.
27. Jung, J. S., Bhat, R. V., Preston, G. M., Guggino, W. B., Baraban, J. M. & Agre, P. (1994) *Proc. Natl. Acad. Sci. USA* **91,** 13052–13056.
28. Amiry-Moghaddam, M., Otsuka, T., Hurn, P. D., Traystman, R. J., Haug, F. M., Froehner, S. C., Adams, M. E., Neely, J. D., Agre, P., Ottersen, O. P. & Bhardwaj, A. (2003) *Proc. Natl. Acad. Sci. USA* **100,** 2106–2111.
29. Newman, E. A. (1986) *Ann. N.Y. Acad. Sci.* **481,** 273–286.
30. Guadagno, E. & Moukhles, H. (2004) *Glia* **47,** 138–149.
31. Amiry-Moghaddam, M. & Ottersen, O. P. (2003) *Nat. Rev. Neurosci.* **4,** 991–1001.
32. Fukuda, S., Fini, C. A., Mabuchi, T., Koziol, J. A., Eggleston, L. L., Jr., & del Zoppo, G. J. (2004) *Stroke* **35,** 998–1004.
33. Ingelsson, M., Fukumoto, H., Newell, K. L., Growdon, J. H., Hedley-Whyte, E. T., Frosch, M. P., Albert, M. S., Hyman, B. T. & Irizarry, M. C. (2004) *Neurology* **62,** 925–931.